Turkish Journal of Electrical Engineering & Computer Sciences

http://journals.tubitak.gov.tr/elektrik/

Research Article

Turk J Elec Eng & Comp Sci
(2019) 27: 11 – 23

doi:10.3906/elk-1803-60

Sensorless second-order switching surface for a three-level boost converter

Tarek MESSIKH*, Nasrudin Abd RAHIM, Saad MEKHILEF
Department of Electrical Engineering, Faculty of Engineering, University of Malaya, Kuala Lumpur, Malaysia

Received: 09.03.2018 • **Accepted/Published Online:** 07.09.2018 • **Final Version:** 22.01.2019

Abstract: This paper proposes a sensorless second-order switching surface to control a three-level boost converter (TLBC). A predictive current method is proposed to reduce the number of sensors in the normal second-order switching surface method. Based on a developed model of the TLBC, the current is estimated and a switching surface is formulated in the state-energy plane. Simulation and hardware tests are carried out to verify the viability and the effectiveness of the proposed control technique. Results obtained show a good performance of the converter in term of DC-bus balancing and fast dynamic response under sudden load change.

Key words: Boundary control, predictive control, second-order switching surface, sensorless current control

1. Introduction

Successful conversion and control of electrical energy using multilevel converters represents a very important field of research due to the rapid growth of power demand with further requirements on power quality and efficiency. To fulfill these demands, new switches, typologies, and control schemes have been developed. Besides that, the controls of these converters have to accomplish crucial roles in optimizing performance and maintaining the desired robustness under various operation conditions [1, 2]. Conventional approaches based on small-signal linear techniques have been found to be unable to achieve the necessary regulation, dynamic response, and required stability for these systems [3]. Therefore, researchers focus on developing some advanced control techniques, which are able to satisfy the complex requirements of power conversion systems. In particular, modern control techniques such as sliding mode control, hysteresis control method, predictive control method, and graphical control method have been applied to these systems. The practicability of these modern methods has been properly investigated in different research works [4–6]. In some recent work, a boundary control (BC) technique with second-order switching surface was investigated and was demonstrated to offer a promising solution for controlling power converters [7, 8].

BC is a geometric-based control approach appropriate for switching converters, which typically has a distinguishing feature of controlling converter operation without differentiating start-up, transient, and steady-state modes. Hence, it has the ability to handle large-signal disturbances in the input and output sides [9]. The concept of the second-order switching surface σ^2 was proposed and applied for buck converters in [10]. It is derived by estimating the state trajectory movement after a switching action, resulting in a high state trajectory velocity along the switching surface. Therefore, the converter reverts to the steady state in two switching actions under large-signal disturbances. Currently, it is applied for all types of converters and the generation of the second-order switching surface is carried out in the state energy plane rather than the state plane [11].

*Correspondence: messikh_tarek@yahoo.fr

The BC technique can ensure system stability and good dynamic performance. However, it will require using numerous sensors, which will affect the cost and the system performance when controlling a three-level boost converter (TLBC). Therefore, it is preferable to adopt some sensorless voltage or current techniques. Many research activities are carried out to propose the diminution of input signals [12, 13]. The reduction of the sensor number is of utmost concern to industrial users due to its significant cost advantage as well as a reliability issue. An interesting approach is to apply a sensorless current mode technique, where the inductor current is estimated from the sensed input and output voltages [14]. This paper presents a BC using a second-order switching surface with a predictive current capability to reduce the number of current sensors used. An accurate model of the converter is developed and used to obtain the mathematical equations that predict the inductor current from the sensed input and output voltages. Then a second-order switching surface is formulated in the state energy plane as described in [11] to control the converter and achieve a balanced output voltage. Besides producing a stable and balanced output voltage, the developed control technique can withstand large-signal disturbances and return rapidly to its steady-state value. The proposed control algorithm is simulated, implemented in TMS320F2812, and tested using prototype hardware. The converter exhibits better results in term of DC-bus balancing and fast dynamic response under sudden load change. Modeling, design, and analysis of the overall system will be given.

2. TLBC mathematical analysis

The circuit configuration of a typical TLBC is shown in Figure 1. This topology has the advantage of less current ripple by around four times if it is compared to the traditional boost converter; hence, the inductance value is less by around four times and so there is high efficiency and low cost. The output voltage of the TLBC is adequately controlled by the switching pair (Q1, Q2), (D1, D2).

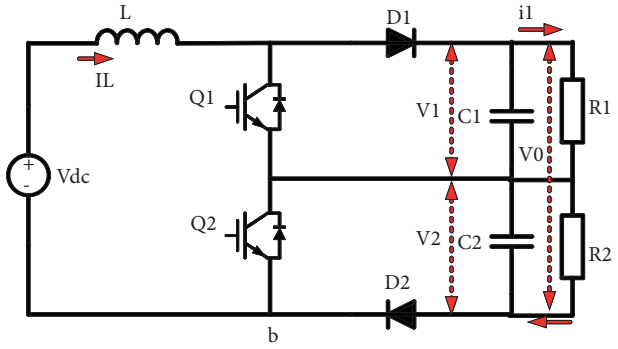

Figure 1. Proposed TLBC topology.

2.1. TLBC working principle

Assuming a balanced voltage output of the converter where V1 is equal to V2, it is basically clear that there are two regions where this converter can operate. The first control region is applied when the input voltage is less than each capacitor output voltage (V_{dc} < V1 & V_{dc} < V2), while the second control region is applied when the input voltage is higher than each capacitor output voltage (V_{dc} > V1 & V_{dc} > V2). Figure 2 illustrates the switching state in each control region. If the TLBC works in region I, the charging voltage is Vdc and the discharging voltage is either (V1-V_{dc}) or (V2-V_{dc}), depending on which boost side is working. Since the upper

and lower capacitors are alternatively used for discharging the inductor voltage, their voltages are theoretically balanced. When the TLBC works in region II, the boost charging mode is either (V_{dc}-V1) or (V_{dc}-V2) and the OFF-mode discharging is (V0-V_{dc}). As this process will be repeated, a balanced output voltage can be achieved. Table 1 summarizes the working principle of this TLBC.

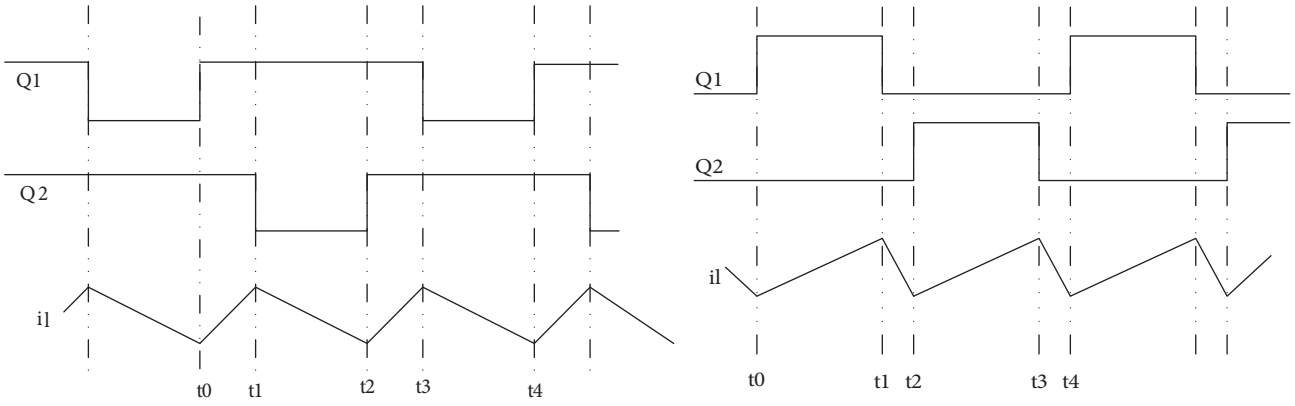

(a) Switching sequence in region I

(b) Switching sequence in region II

Figure 2. Switching sequence for the TLBC.

Table 1. Working principle of the TLBC.

	Satisfied conditions	Boost state	Switches state	
			(Q1, Q2)	(D1, D2)
Region I	Vdc <V1 & Vdc <V2	ON	(1,1)	(0,0)
		OFF	(1,0) or (0,1)	(0,1) or (1,0)
Region II	Vdc >V1 & Vdc >V2	ON	(1,0) or (0,1)	(0,1) or (1,0)
		OFF	(0,0)	(1,1)

2.2. Mathematical model of the TLBC

In order to realize a sensorless control for the TLBC, an accurate modeling system is required. However, for simplification purpose, it is assumed that the TLBC is controlled in region I and works in the continuous current mode to overcome the case where all switches are OFF. With reference to Figure 3, the output voltage of the TLBC is governed by the switching pair (Q1, Q2), (D1, D2), and hence a balanced output voltage can be achieved by operating the converter in Mode 1 and Mode 2 or Mode 1 and Mode 3 simultaneously. Consequently, it is clear that the TLBC is controlled as two conventional boost converters; each one is used to maintain the same output voltage. Therefore, for simplification reasons, the sensorless current control is described only for a simple conventional boost converter and then it will be generalized for the full TLBC. Using the conventional lower boost 1 and neglecting the output voltage of the capacitor C1, the state spaces obtained are:

Mode 1:

$$(Q_1, Q_2) = (1,1) : \begin{bmatrix} \mathrm{i_L} \\ \mathrm{v_2} \end{bmatrix}' = \begin{bmatrix} 0 & 0 \\ 0 & -\frac{1}{RC} \end{bmatrix} \begin{bmatrix} \mathrm{i_L} \\ \mathrm{v_2} \end{bmatrix} + \begin{bmatrix} \frac{1}{L} \\ 0 \end{bmatrix} v_{dc} \tag{1}$$

Mode 2:

$$(Q_1, Q_2) = (1,0) : \begin{bmatrix} \mathrm{i_L} \\ \mathrm{v_2} \end{bmatrix}' = \begin{bmatrix} 0 & -\frac{1}{L} \\ \frac{1}{C} & -\frac{1}{RC} \end{bmatrix} \begin{bmatrix} \mathrm{i_L} \\ \mathrm{v_2} \end{bmatrix} + \begin{bmatrix} \frac{1}{L} \\ 0 \end{bmatrix} v_{dc} \tag{2}$$

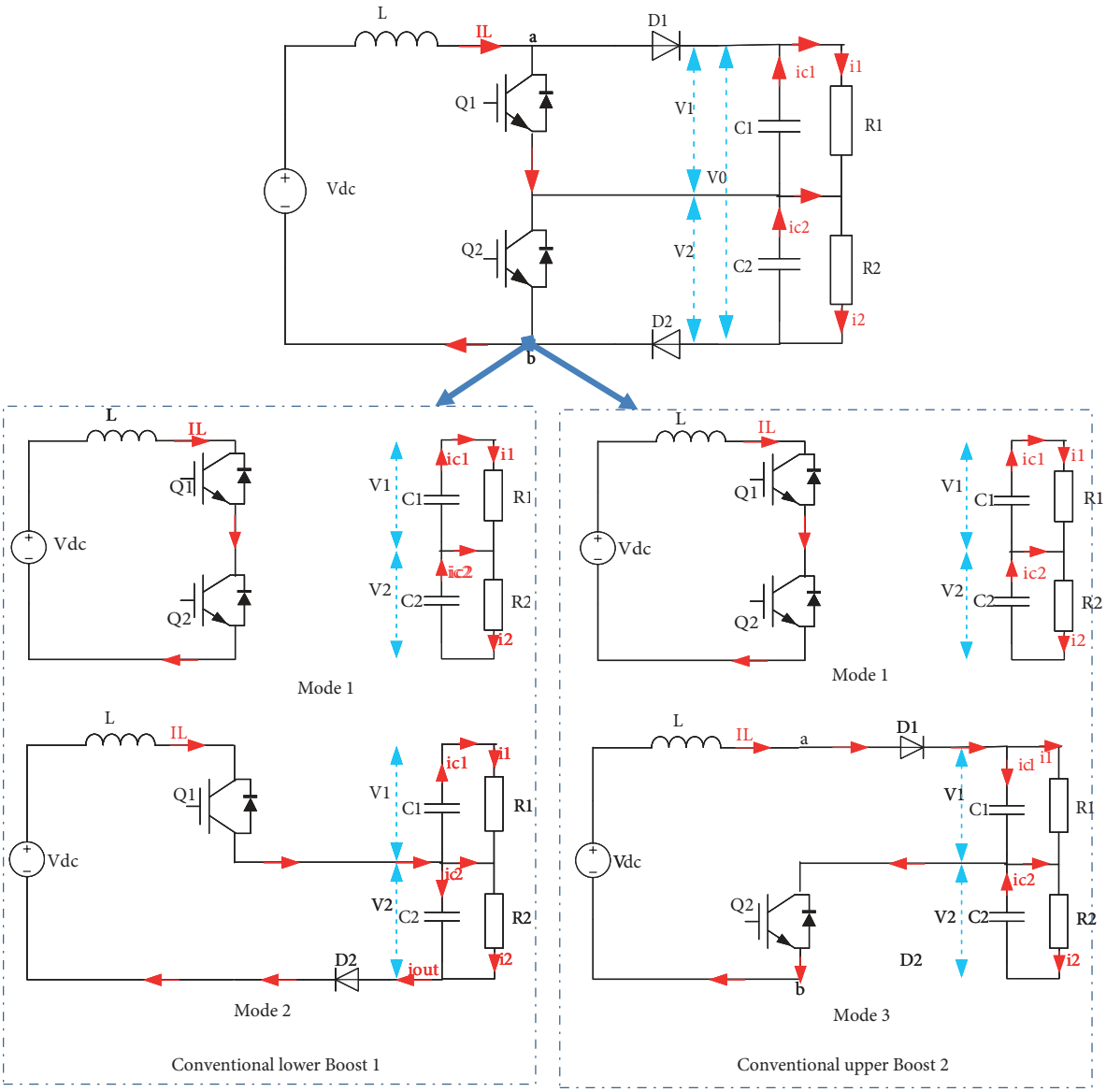

Figure 3. Control of TLBC in region I.

The final approximate model can be written as:

Mode 1:

$$\begin{cases} \text{For} \quad 2a_0h_{on} << 1 \\ I_{on} = i_L\left(t_0\right) + \frac{V_{dc}}{L}h_{on} \\ V_{on} \approx v_2\left(t_0\right) - 2a_0v_0\left(t_0\right)h_{on} \end{cases} \tag{3}$$

Mode 2:

$$\begin{cases} \text{For} \quad \omega_0 h < 0.25 \quad \& \quad a_0 << \omega_0 \\ I_{off} = I_{on} + \frac{V_{dc}-V_{on}}{L}h_{off} \\ V_{off} \approx V_{on} + 0.5\omega_0^2\left(V_{dc} - V_{on}\right)h_{off}^2 + \left(C^{-1}I_{on} - 2a_0V_{on}\right)h_{off} \\ a_0 = \frac{1}{2RC} \\ \omega_0 = \sqrt{\frac{1}{LC} - a_0^2} \end{cases} \tag{4}$$

3. Current estimation method

Using the approximate solution of the TLBC, the estimation of current will be carried out in Mode 1 and Mode 2, respectively. The process of estimation is shown in Figure 4 and explained in detail in the following sections.

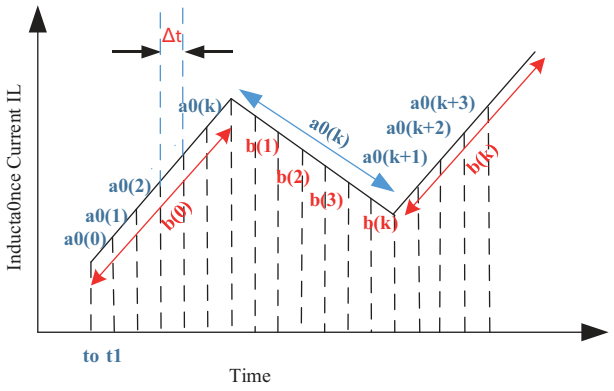

Figure 4. Process of estimating the inductor current.

3.1. Inductor current estimation in Mode 1

A deep analysis of the boost converter's approximate model shows the possibility of estimating the inductor current using only the measurement of the input and output voltages of the converter. To perform this estimation, the time axis is divided into small steps of time with identical durations. The successive activation between the two operating modes is done by assuming a time $t = m\Delta t$ and $m \in N$. In Mode 1, the measured output voltage stated in Eq. (3) is used to estimate the value of a_0 ,ω_0 and the inductor current. The estimation algorithm proposed in Eq. (5) requires only the measurement value of the output voltage at the beginning and the end of each elementary interval, in addition to the interval time $\triangle t$.

$$\begin{cases} a_0\left(k+1\right) = \left(1-\mu\right)a_0\left(k\right) + \mu\frac{1}{2\Delta t}\left(1 - \frac{v_2(k+1)}{v_2(k)}\right) \\ \omega_0\left(k+1\right) = \sqrt{\left(LC\right)^{-1} - a_0(k+1)^2} \\ I\left(k+1\right) = I\left(k\right) + \frac{V_{dc}}{L}\Delta t \\ b\left(k+1\right) = b\left(k\right) \\ I_L\left(k+1\right) = I\left(k+1\right) + b\left(k+1\right) \end{cases} \tag{5}$$

At the end of Mode 1, $v_2\left(k+1\right) = V_{on}$, and $I_l\left(k+1\right) = I_{on}$. If $I\left(1\right) = 0$, $b\left(k\right)$ represents an estimate of the unknown initial value of the inductor current.

3.2. Inductor current estimation in Mode 2

In Mode 2, the converter output voltage given by Eq. (4) is utilized to estimate the inductor current. At this time, a combination between the value of current in Mode 1 with an unknown initial value $b\left(k\right)$ and the output voltage in Mode 2 is made as follows:

$$\begin{cases} I\left(k+1\right) = I\left(k\right) + \frac{V_{dc}-v_2(k)}{L}\Delta t \\ I_L\left(k+1\right) = I\left(k+1\right) + b(k) \\ C\frac{v_0(k+1)-v_2(k)}{\Delta t} + 2a_0\left(k\right)Cv_2\left(k\right) - I\left(k\right) \approx 0.5\omega_0(k+1)^2\,C\left(V_{dc} - v_2\left(k\right)\right)\Delta t + b(k) \end{cases} \tag{6}$$

As $\triangle t$ is small, then the term $\left(0.5\omega_0(k+1)^2 C\left(V_{dc}-v_0\left(k\right)\right)\Delta t\right)$ can be ignored and $b(k)$ can be estimated by:

$$b\left(k+1\right)=\left(1-\mu\right)b\left(k\right)+\mu\left(C\frac{v_2\left(k+1\right)-v_2\left(k\right)}{\Delta t}+2a_0\left(k+1\right)Cv_2\left(k\right)-I\left(k\right)\right) \tag{7}$$

As described in Figure 4, operation in Mode 1 allows us to correctly estimate the value of $a_0(k)$ while Mode 2 permits to estimate the initial value $b(k)$ of the inductor current.

4. Sensorless boundary control of TLBC

The sensorless boundary control of the TLBC can be achieved by combining the current estimation method with the derived second-order switching surface S1. Figure 5 summarizes the proposed sensorless control technique, where only the two output voltages are sensed. The inductor current is predicted in the ON and OFF modes using Eqs. (5) and (6), respectively. We have to mention here that the ON state is (Q1,Q2)=(1,1), and the OFF state is either (Q1,Q2)=(1,0) or (Q1,Q2)=(0,1). After obtaining the needed currents, the control algorithm based on the second-order switching surface derived from the state-energy plane attempts to identify the energy error $\Delta W = W - W_{ref}$ as a quadratic function of the current error by following certain surface forms deduced from the converter operation modes.

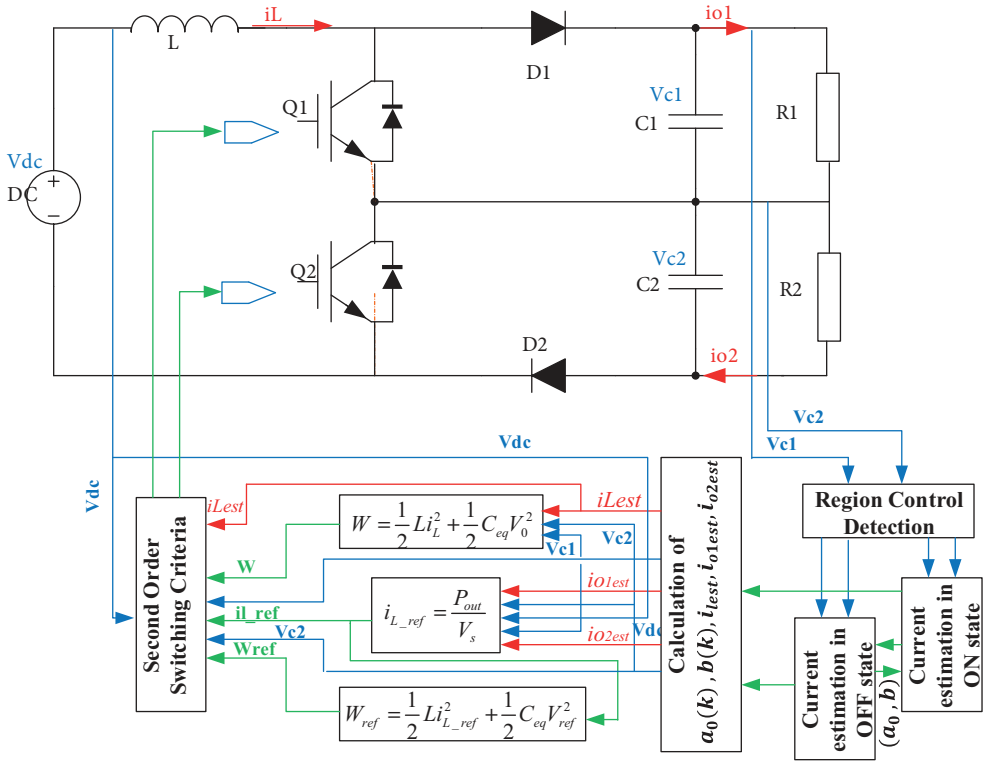

Figure 5. Sensorless boundary control using state energy plane.

Choosing the same capacitance value and the same resistance value in the converter, the instantaneous and reference energies obtained can be expressed based on the total output voltage V_0 and the equivalent

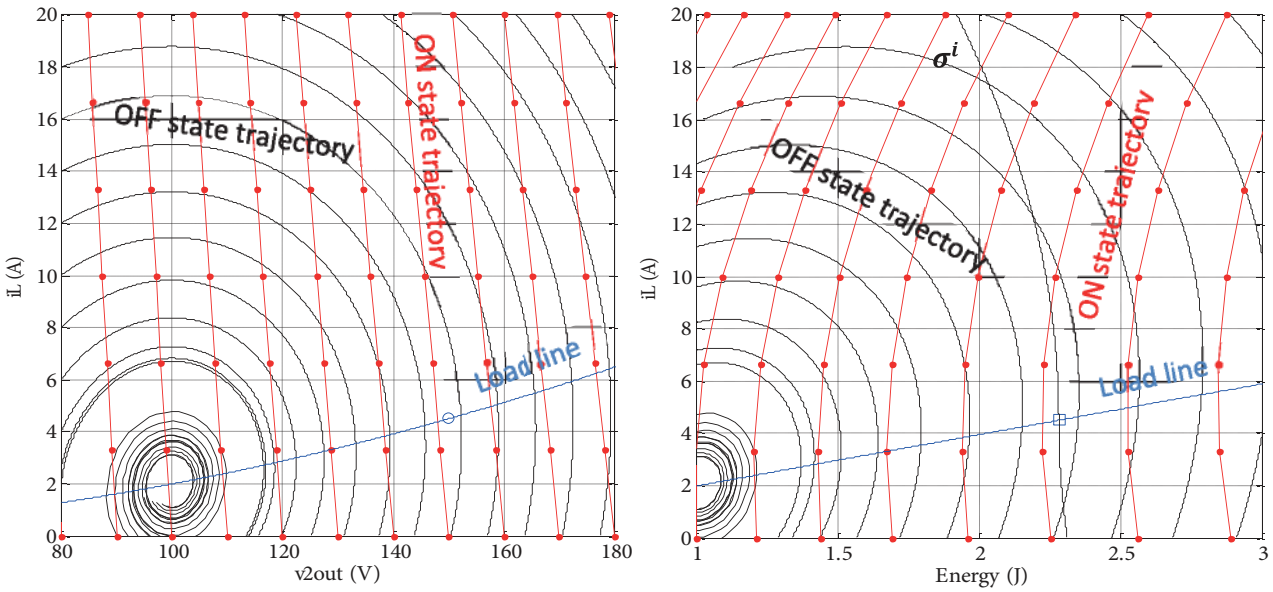

(a) State plane (i_L, v_2) (b) State-energy plane (i_L, w_2)

Figure 6. Switching trajectories for lower boost .

capacitance Ceq as follows:

$$W = \frac{1}{2}Li_L^2 + \frac{1}{2}C_{eq}V_0^2 \tag{8}$$

$$W_{ref} = \frac{1}{2}Li_{L\_ref}^2 + \frac{1}{2}C_{eq}V_0^2 \tag{9}$$

$$i_{L\_ref} = \frac{P_{out}}{V_{dc}} \tag{10}$$

Obtaining the derivation of both W and Wref, then replacing $\frac{di_L}{dt}$ and $\frac{dV_0}{dt}$ by their respective equivalent values, the energy error $\triangle W$ can be expressed as:

$$\Delta W = W - W_{ref} = \int_{t1}^{t2}(dW - dW_{ref})dt = \int_{t1}^{t2}(P_{in} - P_{ref})dt \tag{11}$$

Solving the integral using the trapezoidal method yields:

$$\Delta W = \int_{t1}^{t2} P_{in}dt + \int_{t1}^{t2} P_{ref}dt = (t2 - t1)\frac{P_{in}(t2) + P_{in}(t1)}{2} - P_{ref} \times (t2 - t1) \tag{12}$$

Given that:

$$(t2 - t1) = \frac{P_{in}(t2) - P_{in}(t1)}{dP_{in}} \tag{13}$$

Therefore:

$$\Delta W = \frac{1}{2}\frac{1}{dP_{in}}\left\{(P_{in}(t2) - P_{ref})^2 - (P_{in}(t1) - P_{ref})^2\right\} \tag{14}$$

dP_{in} is determined from the inductor current equation state in each operation mode. For example, in Mode 1, we have:

$$L\frac{di_L}{dt} = V_{dc} \Rightarrow V_{dc}L\frac{di_L}{dt} = V_{dc}^2 \Rightarrow dP_{in} = \frac{V_{dc}^2}{L} \tag{15}$$

As a consequence, the derivation of switching surface criteria for the ON and OFF trajectories can be obtained easily using Eq. (14). The ideal switching surface should traverse the operating point (i_{L_ref}, W_{ref}), traveling the ON-state trajectory when the state is above the load line and traveling the OFF-state trajectory when the state is below the load line. The derived switching surface $S_1(t)$ can be identified as follows:

$$S_1(t) = \begin{cases} 0 \;\; if \;\; \sigma_+^2(t) = \Delta W(t) - k_2[i_L(t) - i_{L\_ref}(t)]^2 > 0 & \& \quad i_L(t) > i_{L\_ref}(t) \\ 1 \;\; if \;\; \sigma_-^2(t) = \Delta W(t) - k_1[i_L(t) - i_{L\_ref}(t)]^2 < 0 & \& \quad i_L(t) < i_{L\_ref}(t) \end{cases} \tag{16}$$

Here, $k_1 = \frac{L}{2}$ and $k_2 = \frac{LV_s}{V_{dc} - v_1}$.

5. Simulation and experimental results

Using MATLAB software the proposed topology is simulated. The control algorithm is implemented following the description shown in Figure 5 and detailed in previous sections. The parameters used are stated in Table 2. As the control of the TLBC is simplified to the control of two conventional boost converters, the state plane of the lower boost and its modification to state-energy plane is displayed in Figure 6. The ON state trajectories are derived by putting (Q1, Q2) = (1, 1) and the OFF trajectories are derived by putting (Q1, Q2) = (1, 0). The simulation results of the control algorithm without using any current sensors are shown in Figure 7. Varying the resistance value from 250 Ω to 125 Ω and vice versa, the results show that the estimation values of $a_0(k)$ and the inductor current i_{L_ref} are almost equal to the real ones. Moreover, the output voltage of each capacitor follows its reference voltage with some differences in the ripple voltage values when the variation occurs. On the other hand, when the control algorithm is compared with current control mode, results are shown in Figure 8. The control of the TLBC with current control mode can be obtained by eliminating the error voltage in S1. The results show that the current control mode has a slower transient response compared with the desired control.

The low power laboratory prototype shown in Figure 9 was built to evaluate the proposed topology performance. The control algorithm that expresses the sensorless boundary control in state-plane energy is implemented in DSP TMS320F2812. A timer interrupt is used to collect the value of voltages from the analog to digital converter (ADC),and then it proceeds with the steps described in the flowchart of Figure 10. The pulses' pattern is generated with a simple function of flip-flop that combines the state of switches in each mode as shown in Table 1. The input voltage is set to 100 V. The results of the total output voltage (Vo), the capacitor C1 voltage (V1),and the pulse of switch Q1 are shown in Figure 11a. The steady-state results satisfy the theoretical study as the converter reached the desired output and the capacitors' voltage are balanced. Furthermore, the start-up of the converter is shown in Figure 11b. An amelioration of the overshoot at the

Table 2. Component values of the TLBC.

Parameter	Value	Parameter	Value
V_{dc}	100 V	C	200 uF
v_{1-ref}	150 V	W	4.50 J
v_{2-ref}	150 V	$\triangle(W)$	0
v_{0-ref}	300 V	k_1	1.5e-3
L	3 mH	k_2	3e-3
R_c	0.2 Ω	R	250 Ω
$\triangle(t)$	50 us	μ	0.9

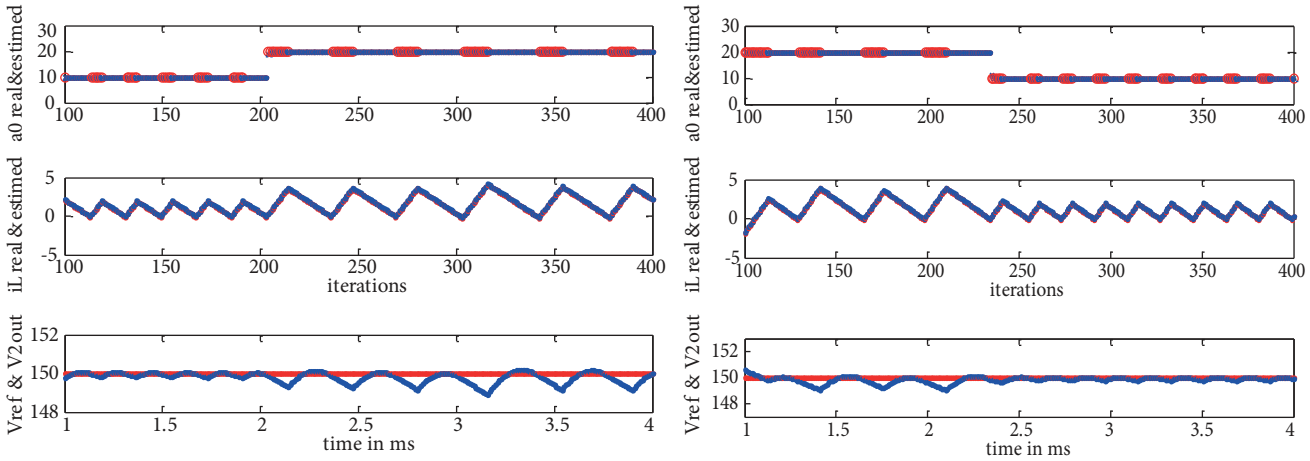

(a) Variation from 250 Ω to 125 Ω

(b) Variation from 125 Ω to 250 Ω

Figure 7. Sensorless control technique verification.

start-up is observed. The converter output reaches the steady-state output voltage at almost 6 ms. The time taken is not only for the purpose of getting the required energy to reach the steady-state value but also related

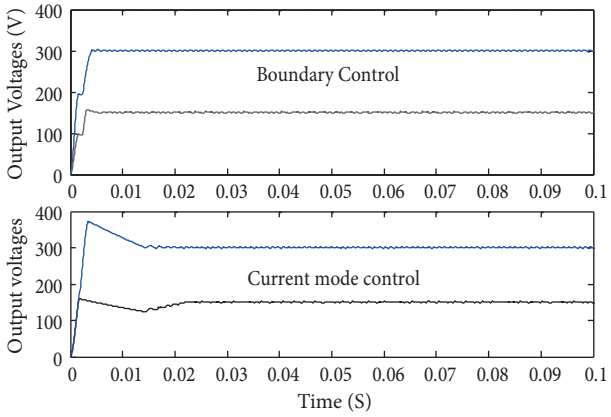

Figure 8. Comparison between two control modes in region 1.

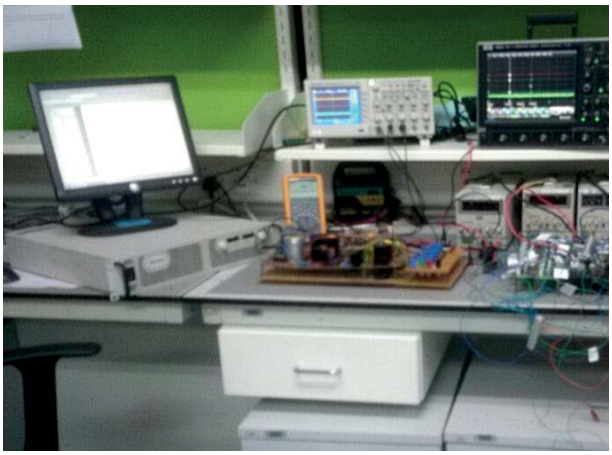

Figure 9. Laboratory prototype.

to the convergence of the sensorless algorithm parameters that estimate the inductor current.

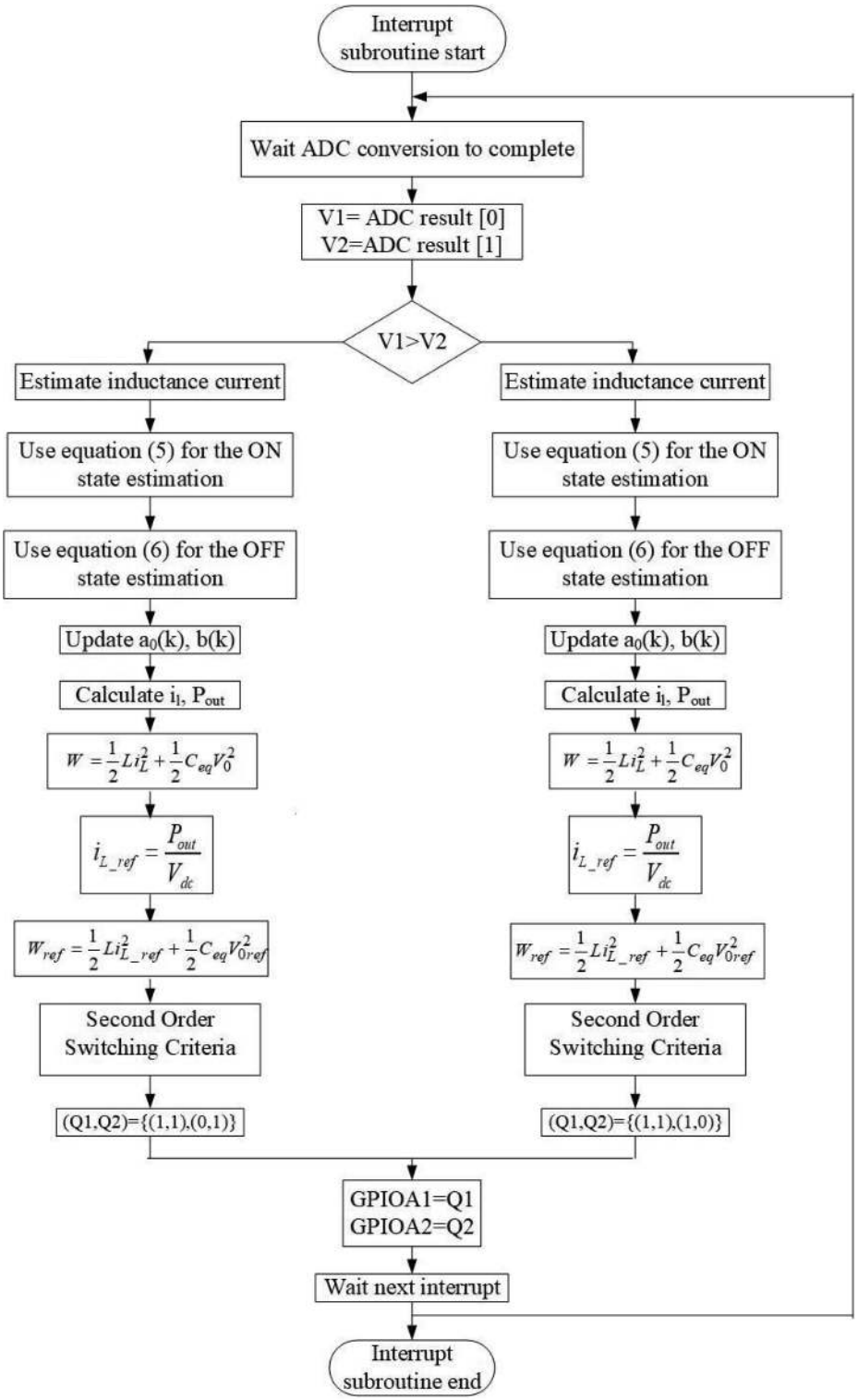

Figure 10. Flowchart of the sensorless control method

Another important parameter to verify is the robustness of the sensorless control technique under 50%

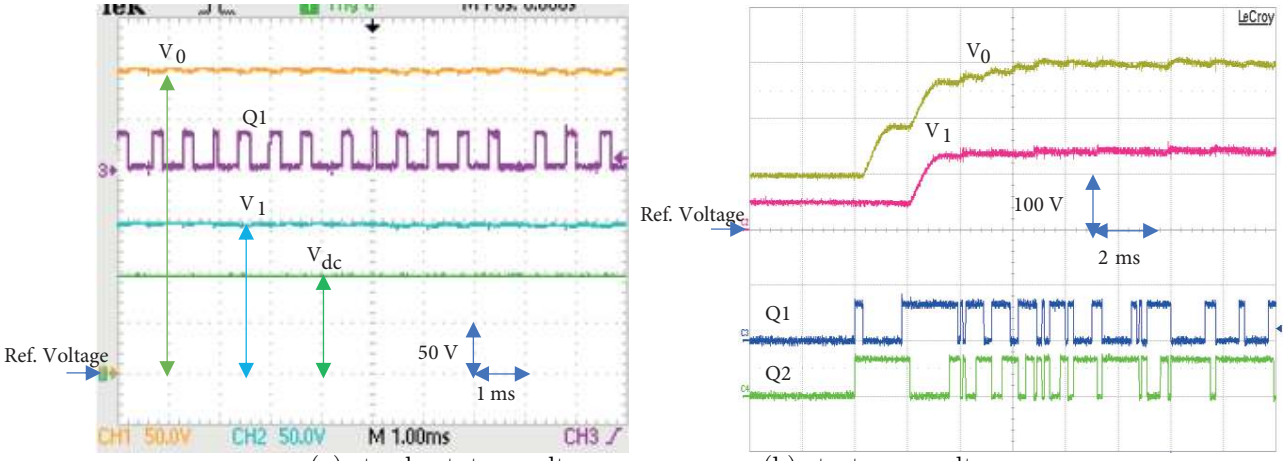

(a) steady state results (b) start up results

Figure 11. TLBC steady state and start-up results.

load change. Referring to Figure 12, the decreasing or increasing of load did not affect the TLBC output voltage much. The system can recover to steady state in a short time with some differences in the ripple voltage. It can also be seen that the generated pulses are different in terms of width to cope with the new reference current generated. As follows, the converter attains the steady state within a few switching cycles. In BC theory, it is important to mention that to limit the switching frequency and to prevent the chattering in the output voltage, a hysteresis band Δw is added into the ideal switching surface σ^2. The steady-state parameters and the stability analysis criteria are defined in Table 3. Regarding the stability of the system, the point along the switching surface σ^2 is characterized into three groups: refractive point, reflective point, and rejective point. These three elements direct the stability of the system. If the switching surfaces are along the boundary of the reflective and refractive regions, the converter will show fast dynamic response.

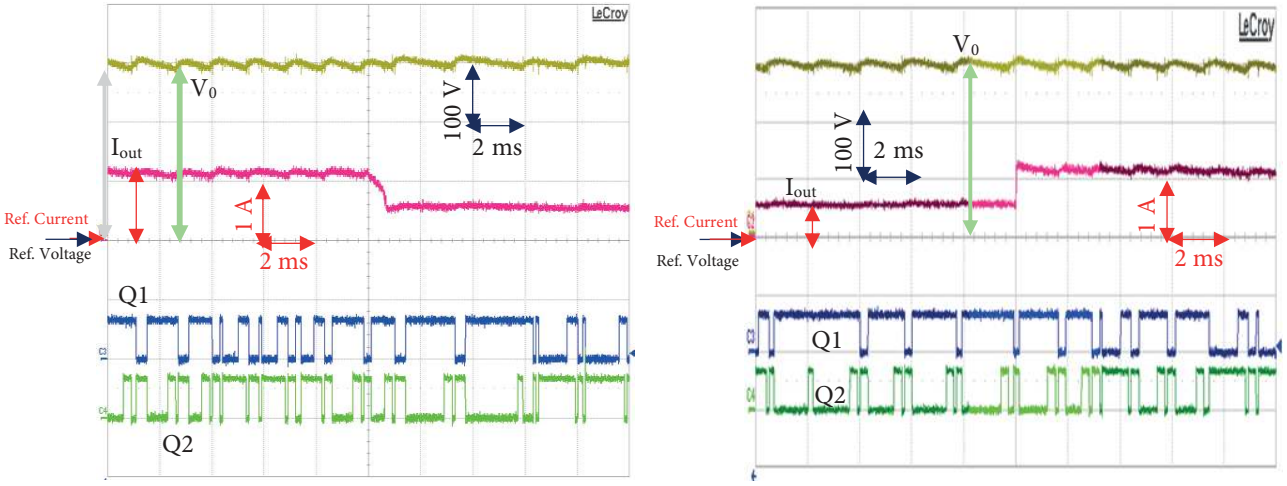

Figure 12. TLBC response under 50% load change. (Vo: 100 V/div, Iout: 1 A/div, Q: 5 V/div, Time: 2 ms/div)

Besides its control technique, this topology has some other benefits if compared to conventional or interleaved boost converters. Table 4 provides a comparison between a conventional boost converter, a two-

Table 3. System analysis of the TLBC.

Steady state analysis	Large signal stability analysis
Current ripple: $\Delta i_{\min} = \Delta i_{\max} = \sqrt{\frac{2}{k_1 - k_2}\Delta w}$	Reflective mode: $k_1 > \frac{L}{2} \quad \& \quad k_2 < \frac{LV_{dc}}{2(V_{dc} - V_0/2)}$
Voltage ripple: $v_{0\min} = \sqrt{\frac{4}{C}W_{ref} + \frac{4}{C}\frac{k_1+k_2}{k_1-k_2}\Delta w - \frac{2L}{C}(i_{L\_ref} + \Delta i_{\max})^2}$ $v_{0\max} = \sqrt{\frac{4}{C}W_{ref} + \frac{4}{C}\frac{k_1+k_2}{k_1-k_2}\Delta w - \frac{2L}{C}L(i_{L\_ref} - \Delta i_{\min})^2}$	Rejective mode: $k_1 < -\frac{L}{2} \quad \& \quad k_2 > \frac{LV_{dc}}{2(V_0/2 - V_{dc})}$
Switching frequency: $f_s = \frac{1}{T_{on}+T_{off}} = \frac{V_{dc}(V_0 - 2V_{dc})}{2LV_0\sqrt{\frac{2}{k_1-k_2}\Delta w}}$	Refractive mode: outside the condition of reflective and rejective mode

interleaved boost converter, and the TLBC. The inductor current ripple in the TLBC is one-fourth that of the conventional one. For the same current ripple, the TLBC requires four times less inductance than the conventional boost converter. As a consequence for the same input current, the inductor size in the TLBC has about one-fourth the size of the inductor in the boost converter. On the other hand, the more competitive counterpart of the TLBC is the two-interleaved boost converter. The input current ripple of the TLBC is the same as that of the two-interleaved boost converter. However, the two-interleaved boost converter has some weaknesses compared to the TLBC, such as it needs two inductors and two controllers with a proper interleaving and current sharing, and in addition the switches have to withstand the full voltage. These drawbacks make the two-interleaved boost converter much less competitive than the TLBC for high power and/or high input voltage.

Table 4. Comparison between some topologies of boost converter.

Boost converter	Interleaved boost converter		TLBC	
	D<0	D>0	Region 1	Region 2
Duty cycle				
$1 - \frac{V_{dc}}{V_0}$	$1 - \frac{V_{dc}}{V_0}$	$1 - \frac{V_{dc}}{V_0}$	$1 - 2\frac{V_{dc}}{V_0}$	$2 - 2\frac{V_{dc}}{V_0}$
Current ripple				
$\frac{V_{dc}D}{f_{sw}L}$	$(\frac{2V_{dc}-V_0}{2Lf_{sw}})(1 - \frac{V_{dc}}{V_0})$	$\frac{V_{dc}(V_0-2V_{dc})}{2Lf_{sw}V_0}$	$\frac{V_{dc}(V_0-2V_{dc})}{Lf_{sw}V_0}$	$\frac{2V_{dc}(V_0-2V_{dc})}{Lf_{sw}V_0}$
Condition for maximum current				
$V_{dc} = 0.5V_0$	$V_{dc} = 0.75V_0$	$V_{dc} = 0.25V_0$	$V_{dc} = 0.25V_0$	$V_{dc} = 0.75V_0$
Maximum current ripple				
$\frac{V_0}{4f_{sw}L}$	$\frac{V_0}{16f_{sw}L}$		$\frac{V_0}{16f_{sw}L}$	

6. Conclusion

A sensorless boundary control of a TLBC in state-energy plane has been proposed. A predictive current control is used to estimate the inductor current needed to formulate the second-order switching surface criteria. This method preserves the good dynamic performance of the normal boundary control without using current sensors. Simulation and experimental results show that the TLBC generates a balanced DC-bus output voltage. Under the sensorless control method, the converter has a fast transient response; the output voltage is usually quickly brought back to steady state during large-signal disturbances. Besides its fast transient response, the control

using second-order switching has improved the overshoot at the start-up. The results obtained demonstrate a similarity between the experimental test and the theoretical investigations.

References

[1] Gaur P, Singh P. Various control strategies for medium voltage high power multilevel converters: a review. In: 2014 Recent Advances in Engineering and Computational Sciences; 6–8 March 2014; Chandigarh, India. New York, NY, USA: IEEE. pp. 1-6.

[2] Guo Z, Sun K. Three level DC-DC converter based on cascaded dual half-bridge converter for circulating loss reduction. In: IEEE 2016 Energy Conversion Congress and Exposition; 18–22 September 2016; Milwaukee, WI, USA. New York, NY, USA: IEEE. pp. 1-8.

[3] Cvetkovic I, Boroyevich D, Mattavelli P, Lee FC, Dong D. Unterminated small-signal behavioral model of DC/DC converters. IEEE T Power Electr 2013; 28: 1870-1879.

[4] Silva FA. Sliding mode control of switching power converters: techniques and implementation [book news]. IEE Ind Electron M 2012; 6: 60-61.

[5] Ruan X, Li B, Chen Q, Tan SC, Tse CK. Fundamental considerations of three-level DC/DC converters: topologies, analyses, and control. IEEE T Circuit-I 2008; 55: 3733-3743.

[6] Schild A, Lunze J, Krupar J, Schwarz W. Design of generalized hysteresis controllers for DC/DC switching power converters. IEEE T Power Electr 2009; 24: 138-146.

[7] He Y, Chung HSH, Ho CNM, Wu W. Direct current tracking using boundary control with second-order switching surface for three-phase three-wire grid-connected inverter. IEEE T Power Electr 2017; 32: 5723-5740.

[8] He Y, Chung HSH, Ho CNM, Wu W. Use of boundary control with second-order switching surface to reduce the system order for deadbeat controller in grid-connected inverter. IEEE T Power Electr 2016; 31: 2638-2653.

[9] Chiu JYC, Leung KKS, Chung HSH. High-order switching surface in boundary control of inverters. In: IEEE 2007 Power Electronics Specialists Conference; 17–21 June 2007; Orlando, FL, USA. New York, NY, USA: IEEE. pp. 2298-2304.

[10] Leung KKS, Chung HSH. Derivation of a second-order switching surface in the boundary control of buck converters. IEEE Power Electronics Letters 2004; 2: 63-67.

[11] Song TT, Chung HSH. Boundary control of boost converters using state-energy plane. IEEE T Power Electr 2008; 23: 551-563.

[12] Chen HC, Lu CY, Li GT, Chen WC. Digital current sensorless control for dual-boost half-bridge PFC converter with natural capacitor voltage balancing. IEEE T Power Electr 2017; 32: 4074-4083.

[13] Tong Q, Zhang Q, Min R, Zou X, Liu Z, Chen Z. Sensorless predictive peak current control for boost converter using comprehensive compensation strategy. IEEE T Ind Electron 2014; 61: 2754-2766.

[14] Tong Q, Chen C, Zhang Q, Zou X. A sensorless predictive current controlled boost converter by using an EKF with load variation effect elimination function. Sensors 2015; 15: 18-25.